Geomechanics and Engineering, *Vol. 35, No. 6 (2023) 627-636*
https://doi.org/10.12989/gae.2023.35.6.627

The influence of fine particle migration on pore structure of overlying ballast under cyclic loading

Yu Ding[1,2,3], Yu Jia*[3], Zhongling Zong[1,2], Xuan Wang[3,4], Jiasheng Zhang[3,4] and Min Ni[1]

[1]*School of Civil and Ocean Engineering, Jiangsu Ocean University, Lianyungang, Jiangsu, 222005, China*
[2]*Jiangsu Ocean Engineering Research Center for Intelligent Infrastructure Construction, Lianyungang, Jiangsu, 222005, China*
[3]*School of Civil Engineering, Central South University, Changsha, Hunan 410083, China*
[4]*National Engineering Research Center of High-speed Railway Construction Technology, Central South University, Changsha, Hunan 410083, China*

(*Received June 7, 2023, Revised November 2, 2023, Accepted November 23, 2023*)

Abstract. The essence of subgrade mud pumping under train load is the migration of fine particles in subgrade soil. The migration of fine particles will change the pore structure of overlying ballast, thus affecting the mechanical properties and hydraulic properties of ballast layer. It is of great theoretical significance and engineering value to study the effect of fine particle migration on the pore structure of ballast layer under cyclic loading. In this paper, a tailor-made subgrade mud pumping test model and an X-ray computed tomography (CT) scanning equipment were used to study the influence of migration of fine particles in subgrade soil on the pore parameters (plane porosity, volume porosity, pore distribution and pore connectivity) of overlying ballast under cyclic loading. The results show that the compression of ballast pores and the blockage of migrated fine particles make the porosity of ballast layer decreases gradually. And the percentage of small pores in ballast layer increases, while the percentage of large pores decreases; the connectivity of pores also gradually decreases. Based on the test results, an empirical model of ballast porosity evolution under cyclic loading is established and verified.

Keywords: cyclic loading; empirical model of porosity evolution; fine particle migration; pore connectivity; pore size distribution; porosity

1. Introduction

Mud pumping under train load is a common subgrade problem in existing railway lines, which is difficult to be cured (Indraratna *et al.* 2010, Saride *et al*. 2013, Chawla *et al.* 2016, Tang *et al.* 2018, Singh *et al.* 2020, Ding *et al*. 2022a). The essence of subgrade mud pumping under train load is the migration of fine particles in subgrade soil (Trani *et al.* 2010a, Trani *et al.* 2010b, Yang *et al.* 2021). The fine particles migrate to the overlying ballast layer, which change the pore structure of the overlying ballast and damage its strength and drainage performance (Indraratna *et al.* 2011, Hussaini *et al.* 2016, Nagrale *et al.* 2017, Nguyen *et al.* 2019, Chen *et al.* 2019). Therefore, it is of great theoretical significance and engineering value to study the influence of fine particle migration on pore structure of overlying ballast layer under cyclic loading.

The microscopic observation methods of soil pore structure mainly include scanning electron microscopy (SEM) (Tang *et al.* 2007, Romero *et al.* 2007), mercury intrusion porosimetry (MIP) method (Romero *et al.* 2007, Wang *et al.* 2020), nuclear magnetic resonance (NMR) method, computed tomography (CT) scanning technology (Zhang 2017) and so on. Among them, CT scanning technology can realize the visualization of soil pore structure without damaging the internal structure of the soil, and it is increasingly applied to geotechnical engineering (Watanabe *et al.* 2012, Mukunoki *et al.* 2016, Dumberry *et al.* 2018). Hamamoto *et al.* (2016) analyzed the changes in pore structure characteristics of sand and glass beads under different compaction degrees by CT scanning technology. They found that the glass beads were easy to form a more continuous and larger pore network under the same porosity, which had a higher permeability. Alshibli *et al.* (2008) studied the changes of shear zone thickness in the process of sand shear and analyzed the pore structure characteristics in shear zone by CT scanning technology. Kim *et al.* (2010) studied the changes of pore structure before and after compaction by CT scanning technology, and found that the number of pores in the sample decreased by 71 % and the porosity decreased by 64 % after compaction. Jiang *et al.* (2019) analyzed the volumetric deformation behavior of crushed stone samples and the particles movement during triaxial compression through the CT scanning technology. Wang *et al.* (2017) conducted a series of dynamic triaxial tests to study the liquefaction characteristics of gravel soil under cyclic loading. Combined with CT scanning technology and discrete element software, they analyzed the microscopic structure changes of gravel soil during liquefaction, and revealed the microscopic mechanism of gravel soil liquefaction. Hall *et al.* (2010) investigated the formation of shear band and the motion (translation and rotation) characteristics of sand particles in the process of triaxial compression test by CT

*Corresponding author, Ph.D. Student
E-mail: jia_yu@csu.edu.cn

ISSN: 2005-307X (Print), 2092-6219 (Online)

Table 1 Physical and mechanical parameters of clay

Materials	G_s	ω_L / %	ω_p / %	$\rho_{d\max}$ / (g/cm^3)	ω_{opt} / %	c/ kPa	φ / °
Clay	2.64	33.42	16.64	1.81	14.7	27.25	24.08

scanning technology and three-dimensional digital image technology. With the help of CT scanning technology, Nguyen *et al.* (2019) analyzed the change of microscopic characteristics (pore structure, pore ratio and intergranular pore ratio), the evolution of fine particle content and the vertical displacement of soil particle during the process of seepage erosion.

At present, CT scanning technology is mainly used to analyze the pore structure of sand and other soils, and there are relatively few studies been done on pore structure of gravel, especially on the change of gravel pore structure caused by the migration of fine particles. In this paper, a series of subgrade mud pumping tests were carried out with a tailor-made mud pumping test model. Combined with an X-ray computed tomography (CT) scanning equipment, the influence of fine particle migration on the pore parameters (plane porosity, volume porosity, pore distribution and pore connectivity) of ballast layer under cyclic loading were analyzed. Based on the results of porosity evolution curves, an empirical model for the evolution of ballast porosity is proposed. This study explores the formation mechanism and development process of subgrade mud pumping from a microscopic view, which provides a basis for prevention and control of subgrade mud pumping.

2. Pore structure evolution test

2.1 Test materials

The clay is used as the subgrade soil, and its mechanical parameters are shown in Table 1. From Table 1 we can see that the clay can be classified as CL-Lean clay. Fig. 1 shows the particle size distribution curve of clay. It can be seen that the particle composition and plasticity index of the clay meet the requirements of soil that prone mud pumping (Nie *et al.* 2018, Leng *et al.* 2018).

The gravel is used to simulate the ballast layer overlying the subgrade, and the specific gravity of gravel is 2.08 g/cm^3. The particle size distribution curve is shown in Fig. 1, with the non-uniformity coefficient C_u = 1.90 and the curvature coefficient C_c = 1.28. The gravel is classified as poorly graded gravel.

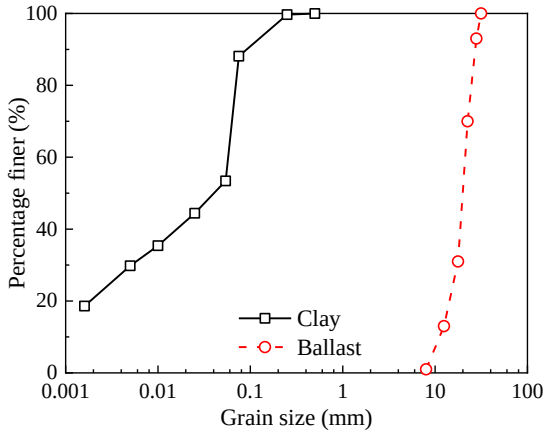

Fig. 1 Particle size distribution curves for clay and ballast

2.2 Test methods

2.2.1 Test model

The tailor-made test model as shown in Fig. 2 is used in the mud pumping test. The model is mainly composed of axial loading device, a visual sample cylinder, a sample saturation device and a data acquisition system. The test model can be used to carry out the mud pumping test of saturated soil under cyclic loading, and the date of axial force and axial displacement during the test can be recorded. More information about the test model can be found in Ding *et al.* (2022b).

A SIEMENS medical CT scanning equipment was used in the CT scanning test, as shown in Fig. 3. The main technical indexes are listed in Table 2.

2.2.2 Testing programs

The diameter of the sample is 178 mm and the height is 180 mm. The lower part of the sample is subgrade soil (clay) and the height is 80 mm. The upper part of the sample is the ballast layer (gravel), with a thickness of 100 mm.

The sample was prepared with a moist compaction method. The initial dry density of clay was controlled to 1.40 g/cm^3, and the moisture content was controlled at the optimal moisture content. The clay was divided into two layers, and the thickness of each layer was 40 mm. Before tamping the next layer, it was necessary to scrape the surface of the compacted clay to ensure a good contact between the layers. The upper gravel of the sample was compacted by two layers, and the thickness of each layer was 50 mm.

After the sample preparation was completed, the sample was saturated. Firstly, the sample was vacuumized, and then the inlet valve at the bottom of the sample was opened, so that the water can slowly flowed into the sample. When the water surface was about 10 mm above the surface of the clay, the inlet valve was closed. After standing for 24 h, the whole sample model was put into the CT scanning equipment for the first CT scanning.

After the first CT scanning, the cyclic load was applied on the sample. The sinusoidal wave was used to simulate the train load, and the amplitudes of the cyclic loading (σ_d) were 50 kPa, 100 kPa and 200 kPa. Before the cyclic loading was applied, the axial static loading (σ_p) of 40 kPa was applied to the sample to simulate the influence of gravity on the subgrade covered by track structure (Bian *et al.* 2016). The loading frequency was 5 Hz (Sun *et al.* 2016), and the loading applied in the test process is shown in Fig. 2.

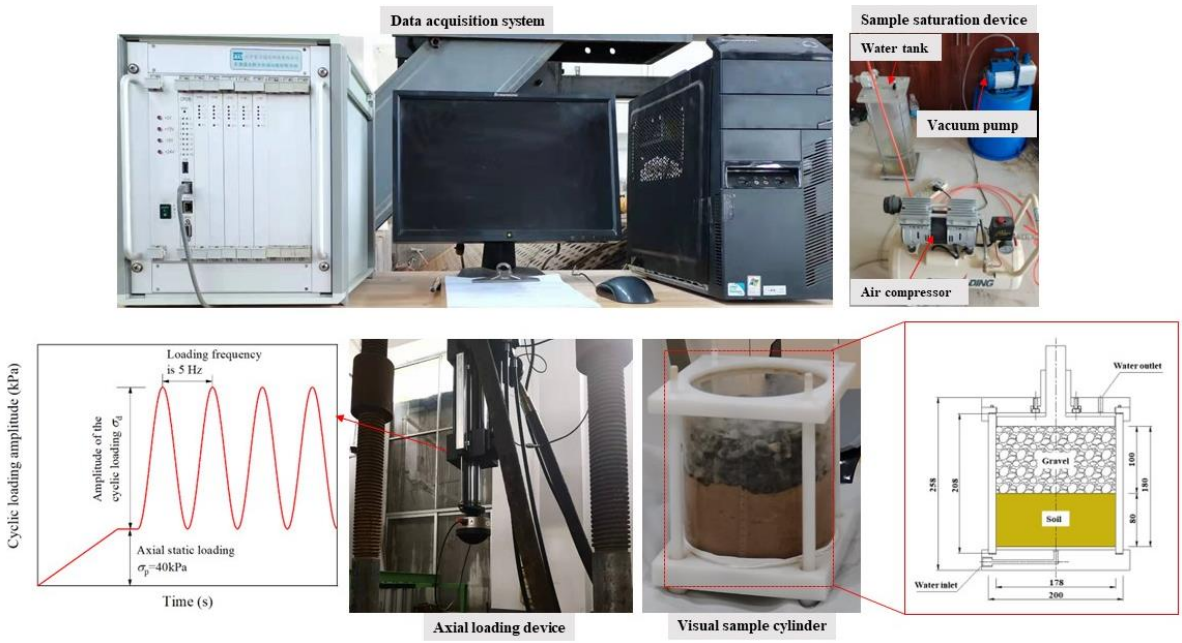

Fig. 2 The test model

Fig. 3 CT scanning equipment

Table 2 Technical indexes of CT scanning equipment

The maximum size of the sample	700 mm×400 mm (diameter × height)
Scanning imaging mode	Spiral scanning
Light source	X-ray
Maximum voltage of light source	120 kV
Spatial resolution	700 μm

When the cycle numbers were 1,000, 15,000, and 30,000, the loading was stopped and the sample was slowly removed from the loading system after standing for a period of time. Then the whole sample was placed in the CT scanning equipment for CT scanning. After scanning, the sample was further loaded until it was loaded to 50,000 times (that is, the end of the test), and then the last CT scanning was performed on the sample. The specific testing programs are shown in Table 3.

3. Test results and analysis

The software of Avizo was used to process CT images. Avizo is a software that can be used for 3D data visualization analysis and modeling. It can realize the processing of CT images, 3D reconstruction, pore microstructure analysis and quantification. The processing of CT images by Avizo mainly includes image noise reduction, image enhancement, image segmentation and image feature extraction. In the process of image segmentation, we adopted a threshold segmentation method. By selecting a suitable threshold gray value (the iterative method is used to determine the threshold value), the particles and pores in the image can be effectively separated and a binary image can be obtained. Then the binary image can be quantitatively analyzed to obtain the pore microparameters such as porosity and pore size distribution.

3.1 Evolution of gravel pore structure during mud pumping

3.1.1 Evolution of porosity

The porosity is divided into plane porosity and volume porosity. Among them, plane porosity is defined as the ratio of pore pixel value to total pixel value in 2D pore mode. Volume porosity (herein after referred to as porosity) is defined as the ratio of pore voxel value to total voxel value in 3D pore model.

Fig. 4 to Fig. 6 show the changes of plane porosity along the gravel height and the changes of gravel porosity for samples S-1.40-50-5, S-1.40-100-5, and S-1.40-200-5 at different loading stages.

As shown in Fig. 4(a), after the sample is saturated, the plane porosity at upper and lower ends the gravel is larger than that at middle of the gravel. The plane porosity fluctuates between 37.63% and 49.55% in the height direction. And the porosity of gravel is 42.32% after saturation.

Table 3 Testing programs

Test No.	Initial dry density of clay ρ_d/(g/cm^3)	Amplitude of cyclic loading σ_d/(kPa)	Frequency f/Hz	Scanning process
S-1.40-50-5	1.40	50	5	The CT scanning was performed at samples after saturation, loaded to 1,000, 15,000, 30,000, and 50,000 cycles, respectively.
S-1.40-100-5	1.40	100	5	
S-1.40-200-5	1.40	200	5	

After 1,000 cycles of loading (as shown in Fig. 4(b)), the plane porosity is large in the upper and middle part, and small in the lower part. Compared with plane porosity of gravel after saturation, the plane porosity of gravel in the same height shows a decreasing trend after 1,000 cycles of loading. The decrease of plane porosity in the upper and middle part of the gravel is mainly caused by the compression of pores in gravel under cyclic loading. The plane porosity of the lower end of the gravel (about 0-8 mm) decreased sharply from about 41% to about 1%, which is mainly caused by blocking effect of fine particles migrated from subgrade under cyclic loading. And the porosity of gravel is 27.33% after 1,000 cycles of loading.

As cyclic loading continues on the sample (as shown in Figs. 4(c) and 4(d)), the plane porosity of the gravel at the same height decreases slightly, and the height of the gravel with a plane porosity close to zero (that is, the height of fine particles migration) gradually increases, and the porosity of the gravel gradually decreases with the increase of loading cycles. Until the end of the test (as shown in Fig. 4(e)), the height of fine particles migration is about 20 mm, and the porosity of the gravel is 16.78%.

For samples S-1.40-100-5 and S-1.40-200-5, the changes of plane porosity and porosity of gravel at different loading stages are consistent with that for sample S-1.40-50-5. That is, after the sample is saturated, the plane porosity at upper and lower ends the gravel is larger than that at middle of the gravel. With the progress of loading, the migrated fine particles gradually blocked the pores in the lower part of gravel, resulting in a large plane porosity in the upper and middle part, and small in the lower part.

In addition, with the increase of loading times, the porosity of the gravel decreases gradually. For sample S-1.40-50-5, the porosity of the gravel is 42.32% after saturation, and the porosity of the gravel is 16.78% at the end of the test, which decreases by about 60%. For sample S-1.40-100-5, the porosity of the gravel is 42.66% after saturation, and the porosity of the gravel is 16.28% at the end of the test, which decreases by about 62%. For sample S-1.40-200-5, the porosity of the gravel is 42.32% after saturation, and the porosity of the gravel is 16.78% at the end of the test, which decreases by about 72%.

3.1.2 Evolution of pore distribution characteristics

The equivalent diameter of pores is usually taken as the basis of pore size classification, and the distribution of pores is counted. In this paper, according to the characteristics of the equivalent diameter of the pores in gravel, the pores with an equivalent diameter less than 3.00 mm are classified as small pores, the pores with a diameter between 3.00 mm and 5.00 mm are classified as medium pores, and the pores with a diameter greater than 5.00 mm are classified as large pores.

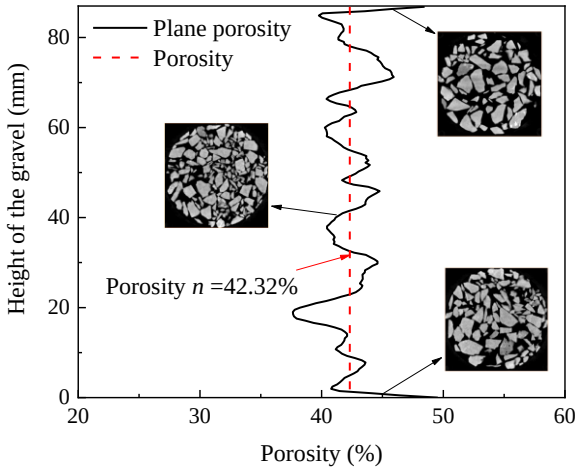

(a) after saturation

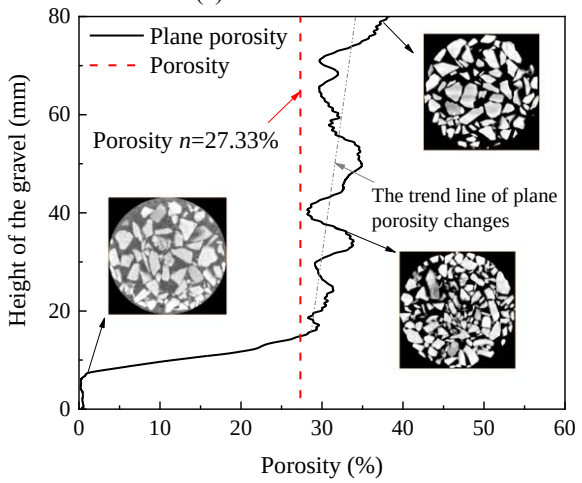

(b) after 1,000 cycles of loading

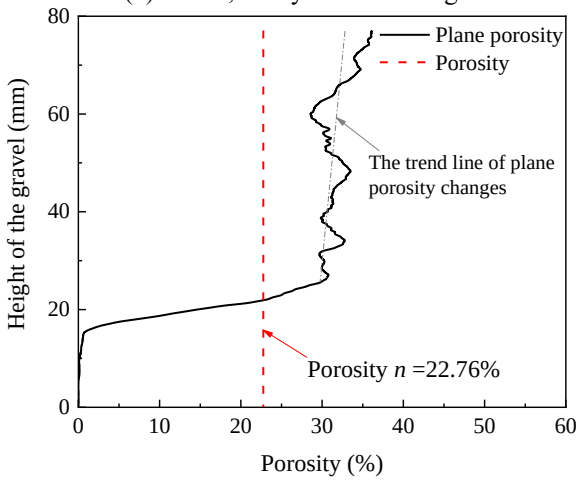

(c) after 15,000 cycles of loading

Fig. 4 The porosity of sample S-1.40-50-5 at different loading stages

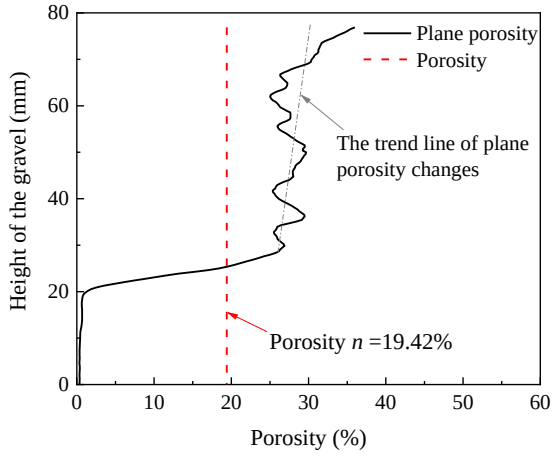

(d) after 30,000 cycles of loading

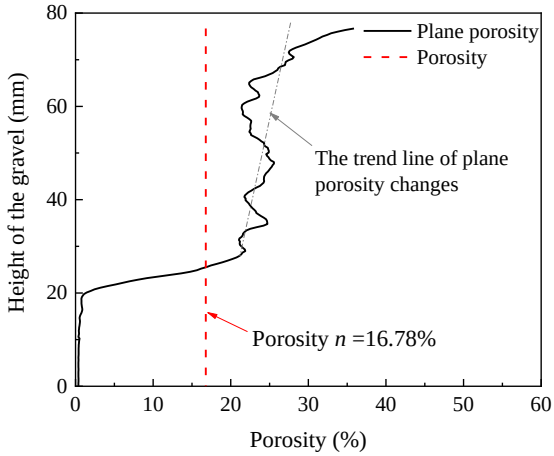

(e) after 50,000 cycles of loading

Fig. 4 Continued-

Fig. 7 shows the gravel pore size distribution of sample S-1.40-50-5 at different loading stages. As shown in Fig. 7(a), after saturation, the equivalent diameter of gravel pores is distributed between 0.90 mm and 16.10 mm, among which the number of pores in the range of 1.00 mm to 2.00 mm is the most, accounting for 38.68% of the total number of pores. The number of pores in the range of 2.00 mm to 3.00 mm and the number of pores less than 1.00 mm account for 19.90% and 18.78% of the total number of pores, respectively. On the whole, the percentage of small pores, medium pores and large pores is 77.36%, 15.40% and 7.24%, respectively. The pore distribution is characterized by more small pores and less large pores. In addition, the pore distribution characteristic curve obeys the lognormal distribution as shown in Eq. (1), and the corresponding lognormal distribution function is shown in Table 4.

$$f(x)=\frac{\alpha}{\sqrt{2\pi}\sigma x}\exp\left(-\frac{(\ln x-\ln x_c)^2}{2\sigma^2}\right) \tag{1}$$

where, x is the pore diameter, α is the relative proportion, x_c is the average pore diameter, σ is the standard deviation.

After cyclic loading is applied on the sample (as shown in Fig. 7(b) to Fig. 7(d)) and at the end of test (as shown in Fig. 7(e)), the equivalent diameter of the gravel pores was distributed within the range of 0 mm to 10.0 mm, and the pores distribution still shows the characteristics of more small pores and fewer large pores. The pore distribution characteristic curve follows the lognormal distribution, and the corresponding lognormal distribution function is shown in Table 4.

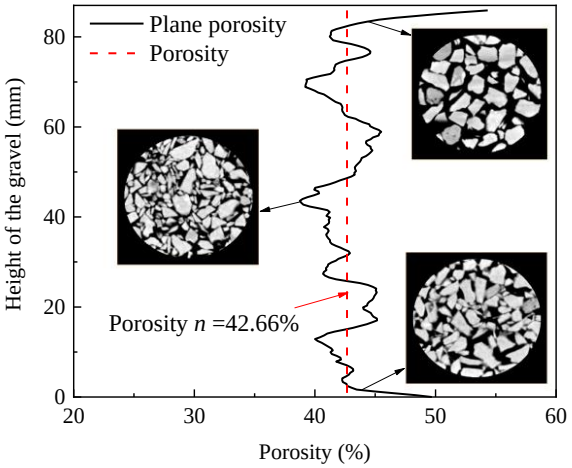

(a) after saturation

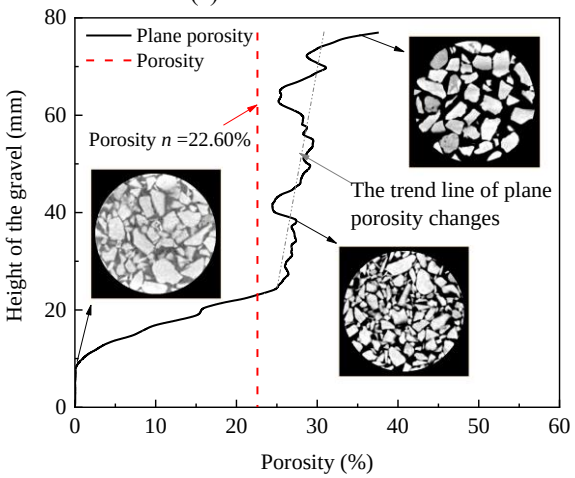

(b) after 1,000 cycles of loading

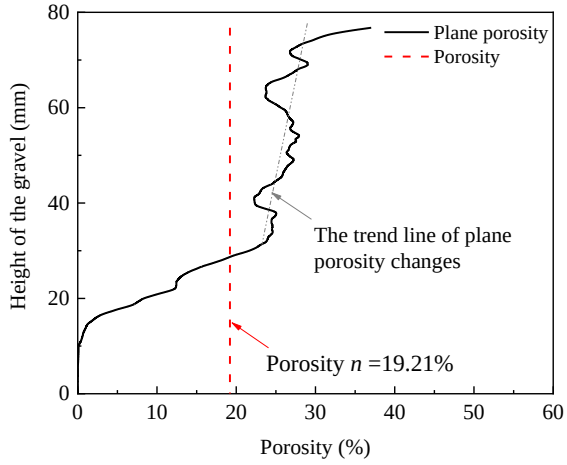

(c) after 15,000 cycles of loading

Fig. 5 The porosity of sample S-1.40-100-5 at different loading stages

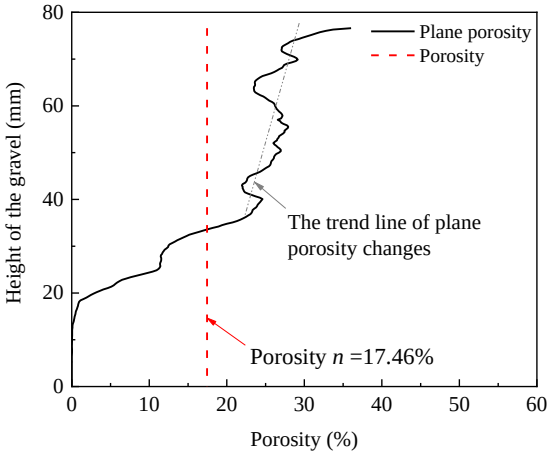

(d) after 30,000 cycles of loading

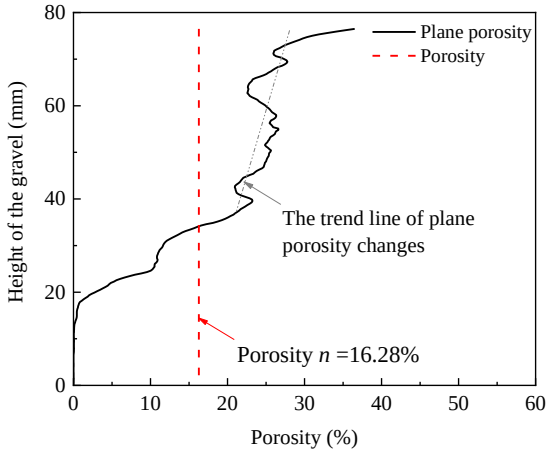

(e) after 50,000 cycles of loading

Fig. 5 Continued-

Fig. 8 shows the curves of the percentage of large, medium and small pores in sample S-1.40-50-5 with cycle number. It can be seen that the percentage of small gravel pores increases with the increase of cycle number, from 77.36% to 82.18%. The percentage of large gravel pores decreases, from 7.22% to 4.70%. And the percentage of medium gravel pores fluctuates with the increase of cycle number. This also indicates that in the process of cyclic loading, the large pores in gravel trends to be compressed or blocked by migrated fine particles and converted into small pores.

For samples S-1.40-100-5 and S-1.40-200-5, the distribution characteristics of pore size and the curves of percentage of gravel pores with cycle number are basically the same as those of sample S-1.40-50-5. Due to space limitation, no further details are required.

3.1.3 Evolution of pore connectivity

The pore connectivity is an important index to evaluate the hydraulic properties of porous media. Pore connectivity is defined as the ratio of the volume of pores through the upper interface to the lower interface to the volume of total pores. That is

$$R_c = \frac{n_c}{n} \times 100\% \quad (2)$$

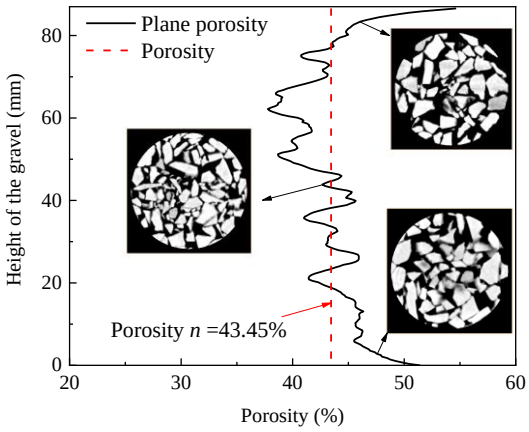

(a) after saturation

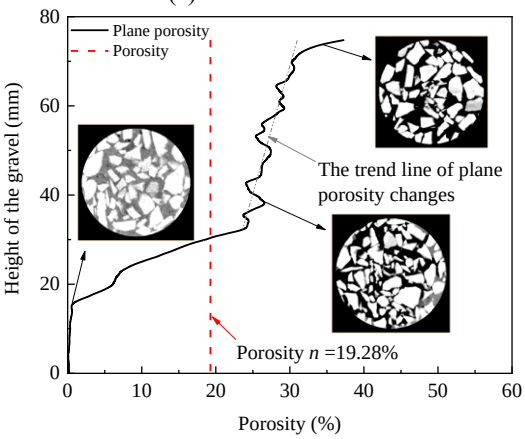

(b) after 1,000 cycles of loading

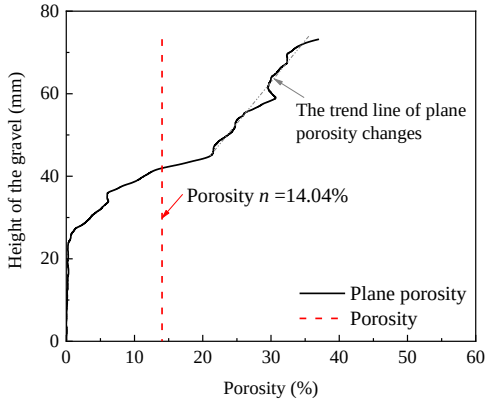

(c) after 15,000 cycles of loading

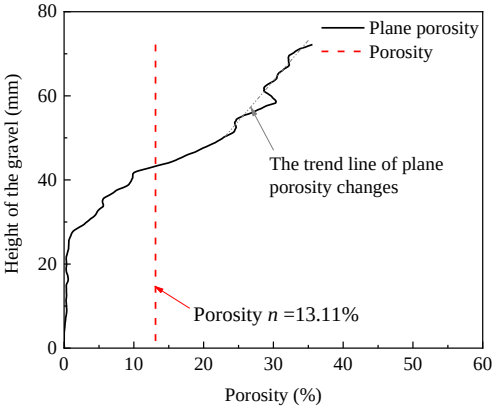

(d) after 30,000 cycles of loading

Fig. 6 The porosity of sample S-1.40-200-5 at different loading stages

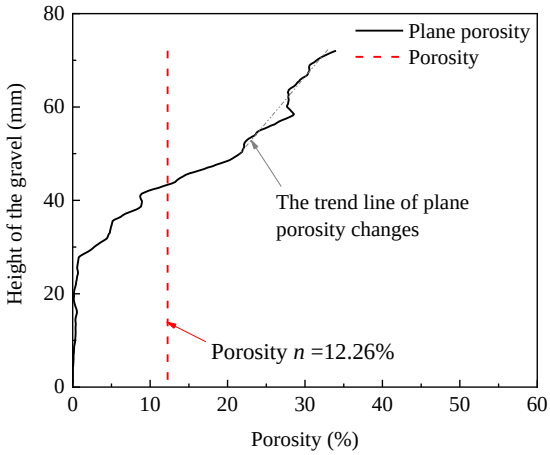

(e) after 50,000 cycles of loading

Fig. 6 Continued-

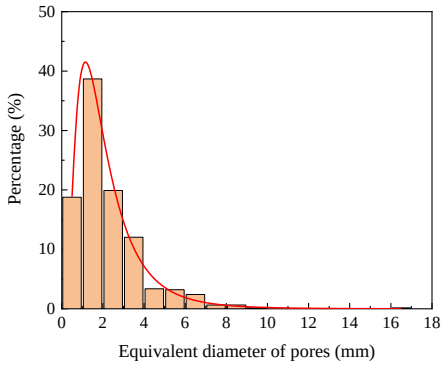

(a) after saturation

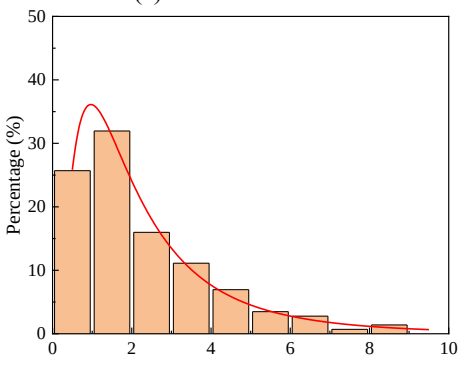

(b) after 1,000 cycles of loading

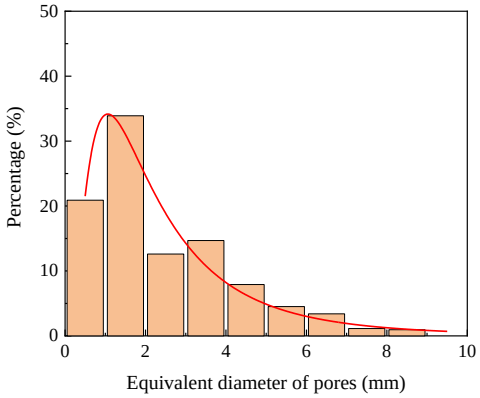

(c) after 15,000 cycles of loading

Fig. 7 Pore size distribution of sample S-1.40-50-5 at different loading stages

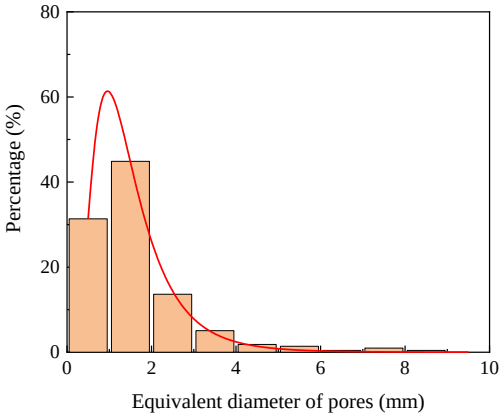

(d) after 30,000 cycles of loading

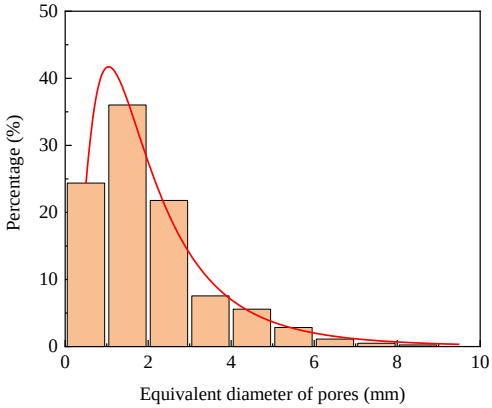

(e) after 50,000 cycles of loading

Fig. 7 Continued-

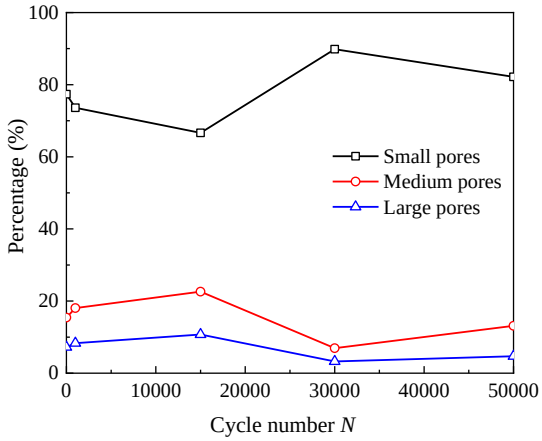

Fig. 8 The curves of percentage of gravel pores with cycle number in sample S-1.40-50-5

where, R_c is pore connectivity, n_c is connected porosity, and n is porosity.

There is little possibility for pores connecting the upper and lower interfaces in the full-size 3D reconstruction model of gravel pores, especially when the fine particles migrated and blocked in the gravel pores. However, in a certain area of the gravel, there are pores connecting the upper and lower interfaces, and the connected pores within the regional gravel also have an important impact on the hydraulic characteristics of gravel layer. Therefore, this paper adopts the method of taking the average value of local

Table 4 Lognormal distribution function of pore size of sample S-1.40-50-5 at different loading stages

Loading stages	α	x_c	σ	R^2
After saturation	99.47	1.79	0.66	0.98
After 1,000 cycles of loading	97.72	1.85	0.81	0.99
After 15,000 cycles of loading	97.26	1.97	0.79	0.98
After 50,000 cycles of loading	97.13	1.32	0.56	0.98
At the end of the test	99.89	1.73	0.71	0.95

pore connectivity instead of the pore connectivity of the whole gravel layer. It is considered an approximate method that can be accepted with some error.

Table 5 to Table 7 show the pore connectivity of samples S-1.40-50-5, S-1.40-100-5 and S-1.40-200-5 under different loading states. As can be seen from Table 5 to Table 7, the pore connectivity of gravel decreases gradually with cyclic loading, and the reduction rate of pore connectivity decrease gradually. For example, in sample S-1.40-50-5 (as shown in Table 5), after saturation, the pore connectivity in gravel is about 84.85%. Under cyclic loading, the migrated fine particles from subgrade soil blocking the pores at the lower part of gravel layer, resulting in the decline of pore connectivity. After 1000 cycles loading, the pore connectivity is 69.61%; after 15,000 cycles loading, the pore connectivity becomes 61.72%; after 30,000 cycles loading, the pore connectivity is 57.84%; and after the test, the pore connectivity is 55.89%.

Table 5 Pore connectivity of sample S-1.40-50-5 at different loading stages

Loading stages	Pore connectivity (%)
After saturation	84.85
After 1,000 cycles of loading	69.61
After 15,000 cycles of loading	61.72
After 50,000 cycles of loading	57.84
At the end of the test	55.89

Table 6 Pore connectivity of sample S-1.40-100-5 at different loading stages

Loading stages	Pore connectivity (%)
After saturation	81.89
After 1,000 cycles of loading	57.17
After 15,000 cycles of loading	51.21
After 50,000 cycles of loading	45.22
At the end of the test	41.58

Table 7 Pore connectivity of sample S-1.40-200-5 at different loading stages

Loading stages	Pore connectivity (%)
After saturation	80.51
After 1,000 cycles of loading	49.63
After 15,000 cycles of loading	36.61
After 50,000 cycles of loading	33.02
At the end of the test	31.13

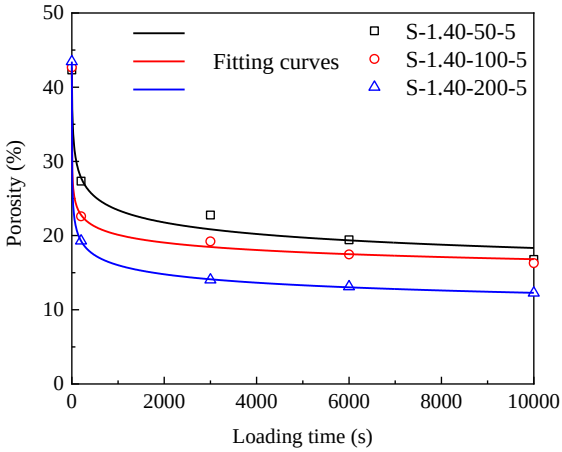

Fig. 9 Curves of gravel porosity with loading time

4. Porosity evolution model

4.1 The establishment of porosity evolution model

The porosity of gravel is significantly changed by migrated fine particles under cyclic loading, and the evolution of porosity is important for the study of mechanical and hydraulic properties of gravel. Based on the CT scanning test results, the changes of gravel porosity with different loading time were analyzed, as shown in Fig. 9. Fig. 9 indicates that the porosity of gravel shows a non-linear decreasing with the increase of loading time, and the reduction rate decreases gradually. The gravel porosity evolution curve caused by migrated fine particles under cyclic loading can be characterized by power function. Based on this, an empirical model of gravel porosity evolution is proposed, as shown in Eq. (3).

$$n = a(t-b)^c \tag{3}$$

where, n is gravel porosity, t is loading time, and a, b, c are fitting parameters.

The empirical model (3) was used to fit the test results, the fitting parameters and the correlation coefficient were obtained, which listed in Table 8. From Table 8, we know that correlation coefficients are all greater than 0.95, which indicating that the empirical model (3) can well predict the evolution trend of the gravel porosity in the process of fine particles migration under cyclic loading.

4.2 The Validation of porosity evolution model

To verify the accuracy of the porosity empirical model

Table 8 Parameters for porosity evolution model (3)

Test No.	Parameters			Correlation coefficient R^2
	a	*b*	*c*	
S-1.40-50-5	49.09	-4.01	-0.11	0.97
S-1.40-100-5	34.38	-0.06	-0.08	0.99
S-1.40-200-5	35.48	-0.17	-0.12	0.99

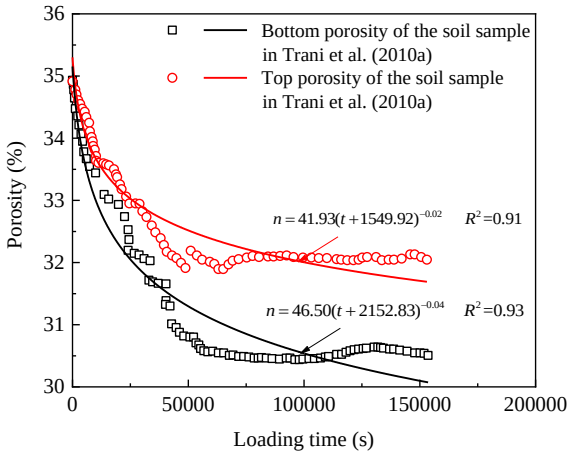

Fig. 10 Validation of porosity evolution model (3)

(3) established in this paper, the experimental data of porosity and time in Trani *et al.* (2010a) were used, and the results were shown in Fig. 10. As can be seen from Fig. 10, the porosity evolution model (3) proposed in this paper can well predict the porosity change curve over time in Trani *et al.* (2010a), and the correlation coefficients are all above 0.90, which verifies the accuracy and applicability of the porosity evolution model (3) proposed in this paper.

5. Conclusions

In this paper, the Computed Tomography (CT) scanning technology was used to study the characteristics of gravel pore structure evolution considering the fine particles migration under cyclic loading. The main conclusions are as follows:

1) After the sample saturation, the plane porosity at upper and lower ends the gravel is larger than that at middle of the gravel. With the application of cyclic loading, the plane porosity of gravel along the height is large in the upper and middle part, and small in the lower part. The porosity of gravel decreases gradually with the application of cyclic loading. For example, after saturation, the porosity of gravel is about 42%; after the test is finished, the porosity of gravel decreases to 16.78% (S-1.40-50-5), 16.28% (S-1.40-100-5) and 12.26% (S-1.40-200-5), respectively.

2) The pore size distribution of gravel is characterized by more small pores and less large pores, and the pore distribution characteristic curve obeys lognormal distribution. With the application of cyclic loading, the large pores in gravel are compressed or blocked by migrated fine particles and transformed into small pores, the percentage of small pores gradually increases, and the percentage of large pores gradually decreases.

3) The pore connectivity of gravel decreases gradually with cyclic loading, but the reduction rate decreases gradually.

4) The porosity of gravel exhibits a non-linear decreasing with increasing loading time, and the rate of decrease gradually slows down. Based on curves of gravel porosity with loading time, an empirical model of gravel porosity evolution is proposed.

Acknowledgments

The study was supported by the National Natural Science Foundation of China (51978674), Science and Technology Research and Development Program of China National Railway Group Corporation Limited (L2022G002), and Innovation and Entrepreneurship Training Program for College Students in Jiangsu Province (202311641122Y). The laboratory tests were performed in the National Engineering Research Center of High-speed Railway Construction Technology with significant support from Dr. Zhang of Central South University. The authors are grateful for the anonymous reviewers for their constructive comments and suggestions.

Conflict of interest

The authors declare that they have no conflict of interest.

References

Alshibli, K.A. and Hasan, A. (2008), "Spatial variation of void ratio and shear band thickness in sand using X-ray computed tomography", *Geotechnique*, **58**(4), 249-257. https://doi.org/10.1680/geot.2008.58.4.249.

Bian, X.C., Jiang, J.Q., Jin, W.F., Sun, D.D., Li, W. and Li, X.M. (2016), "Cyclic and postcyclic triaxial testing of ballast and subballast", *J. Mater. Civil Eng.*, **28**(7), 04016032. https://doi.org/10.1061/(ASCE)MT.1943-5533.0001523.

Chawla, S. and Shahu, J.T. (2016), "Reinforcement and mud-pumping benefits of geosynthetics in railway tracks: Numerical analysis", *Geotext. Geomembranes*, **44**(3), 344-357. https://doi.org/10.1016/j.geotexmem.2016.01.006.

Chen, B., Sun, D.A. and Jin, P. (2019), "Experimental study of the effect of microstructure on the permeability of saturated soft clays", *Geomech. Eng.*, **18**(1), 49-58. https://do.org/10.12989/gae.2019.18.1.049.

Ding, Y., Jia, Y., Wang, X., Zhang, J.S., Luo, H., Zhang, Y. and Chen, X.B. (2022a), "The characteristics of subgrade mud pumping under various water level conditions", *Geomech. Eng.*, **30**(2), 201-210. https://doi.org/10.12989/gae.2022.30.2.201.

Ding, Y., Jia, Y., Wang, X., Zhang, J.S., Chen, X.B., Luo, H. and Zhang, Y. (2022b), "Influence of particle size distribution and initial dry density on the characteristics of subgrade mud pumping", *Rock Soil Mech.*, **43**(9), 2539-2549. https://doi.org/10.16285/j.rsm.2021.1971.

Dumberry, K., Duhaime, F. and Ethier, Y.A. (2018), "Erosion monitoring during core overtopping using a laboratory model with digital image correlation and X-ray microcomputed tomography", *Can. Geotech. J.*, **55**(2), 234-245.

https://doi.org/10.1139/cgj-2016-0684.

Hall, S.A., Bornert, M., Desrues, J., Pannier, Y., Lenoir, N., Viggiani, G. and Bésuelle, P. (2010), "Discrete and continuum analysis of localised deformation in sand using X-ray CT and volumetric digital image correlation", *Geotechnique*, **60**(5), 315-322. https://doi.org/10.1680/geot.2010.60.5.315.

Hamamoto, S., Moldrup, P., Kawamoto, K., Sakaki, T., Nishimura, T. and Komatsu, T. (2016), "Pore network structure linked by X-ray CT to particle characteristics and transport parameters", *Soils Found.*, **56**(4), 676-690. https://doi.org/10.1016/j.sandf.2016.07.008.

Hussaini, S.K.K., Indraratna, B. and Vinod, J.S. (2016), "A laboratory investigation to assess the functioning of railway ballast with and without geogrids", *Transport. Geotech.*, **6**, 45-54. https://doi.org/10.1016/j.trgeo.2016.02.001.

Indraratna, B., Ngo, N.T. and Rujikiatkamjorn, C. (2011), "Behavior of geogrid-reinforced ballast under various levels of fouling", *Geotext. Geomembranes*, **29**(3), 313-322. https://doi.org/10.1016/j.geotexmem.2011.01.015.

Indraratna, B., Rujikiatkamjorn, C., Ewers, B. and Adams, M. (2010), "Class A prediction of the behavior of soft estuarine soil foundation stabilized by short vertical drains beneath a rail track", *J. Geotech. Geoenviron. Eng.*, **136**, 686-696. https://doi.org/10.1061/(ASCE)GT.1943-5606.0000270.

Jiang, J.S., Lin, C., Cheng, Z.L. and Zuo, Y.Z. (2019), "Investigation of macroscopic and microscopic behavior of gravels using triaxial compression test with CT scan", *J. Test. Eval.*, **47**(6), 15. https://doi.org/10.1520/JTE20180547.

Kim, H., Anderson, S.H., Motavalli, P.P. and Gantzer, C.J. (2010), "Compaction effects on soil macropore geometry and related parameters for an arable field", *Geoderma*, **160**(2), 244-251. https://doi.org/10.1016/j.geoderma.2010.09.030.

Leng, W.M., Su, Y., Teng, J.D., Nie, R.S. and Zhao, C.Y. (2018), "Analysis and evaluation on physical characteristics of fine-grained soils prone to mud pumping", *J. China Railway Soc.*, **40**(1), 116-122. https://doi.org/10.3969/j.issn.1001-8360.2018.01.018.

Mukunoki, T., Miyata, Y., Mikami, K. and Shiota, E. (2016), "X-ray CT analysis of pore structure in sand", *Solid Earth*, **7**(3), 929-942. https://doi.org/10.5194/se-7-929-2016.

Nagrale, P.P. and Patil, A.P. (2017), "Improvement in engineering properties of subgrade soil due to stabilization and its effect on pavement response", *Geomech. Eng.*, **12**(2), 257-267. https://doi.org/10.12989/gae.2017.12.2.257.

Nguyen, C.D., Benahmed, N., Andò, E., Sibille, L. and Philippe, P. (2019), "Experimental investigation of microstructural changes in soils eroded by suffusion using X-ray tomography", *Acta Geotechnica*, **14**, 749-765. https://doi.org/10.1007/s11440-019-00787-w.

Nguyen, T.T., Indraratna, B., Kelly, R., Phan, N.M. and Haryono, F. (2019), "Mud pumping under railtracks: mechanisms, assessments and solutions", *Australian Geomech. J.*, **54**(4), 59-80.

Nie, R.S., Leng, W.M., Su, Y. and Guo, Y.P. (2018), "Physical and mechanical properties of mud pumping soils in railway subgrade bed", *J. Southwest Jiaotong Univ.*, **53**(2), 286-295. https://doi.org/10.3969/j.issn.0258-2724.2018.02.010.

Romero, E. and Simms, P.H. (2008), "Microstructure investigation in unsaturated soils: a review with special attention to contribution of mercury intrusion porosimetry and environmental scanning electron microscopy", *J. Geotech. Geol. Eng.*, **26**(6), 705-727. https://doi.org/10.1007/s10706-008-9204-5.

Saride, S., Pradhan, S., Sitharam, T.G. and Puppala, A.J. (2013), "Numerical analysis of geocell reinforced ballast overlying soft clay subgrade", *Geomech. Eng.*, **5**(3), 263-281. http://doi.org/10.12989/gae.2013.5.3.263.

Singh, R.P., Nimbalkar, S., Singh, S. and Choudhury, D. (2020), "Field assessment of railway ballast degradation and mitigation using geotextile", *Geotext. Geomembranes*, **48**(3), 275-283. https://doi.org/10.1016/j.geotexmem.2019.11.013.

Sun, Q.D., Indraratna, B. and Nimbalkar, S. (2016), "Deformation and degradation mechanisms of railway ballast under high frequency cyclic loading", *J. Geotech. Geoenviron. Eng.*, **142**(1), 04015056. https://doi.org/10.1061/(ASCE)GT.1943-5606.0001375.

Tang, C.S., Shi, B., Gao, W., Chen, F.J. and Cai, Y. (2007), "Strength and mechanical behavior of short polypropylene fiber reinforced and cement stabilized clayey soil", *Geotext. Geomembranes*, **25**(3), 194-202. https://doi.org/10.1016/j.geotexmem.2006.11.002.

Tang, L.S., Chen, H.K., Sun, Y.L., Zhang, Q.H. and Liao, H.R. (2018), "Traffic-load-induced dynamic stress accumulation in subgrade and subsoil using small scale model tests", *Geomech. Eng.*, **16**(2), 113-124. http://doi.org/10.12989/gae.2018.16.2.113.

Trani, L.D.O. and Indraratna, B. (2010a), "Assessment of subballast filtration under cyclic loading", *J. Geotech. Geoenviron. Eng.*, **136**(11), 1519-1528. https://doi.org/10.1061/(ASCE)GT.1943-5606.0000384.

Trani, L.D.O. and Indraratna, B. (2010b), "Experimental investigations into subballast filtrations behaviour under cyclic conditions", *Australian Geomech.*, **45**(3), 123-133.

Wang, J.D., Li, P., Ma, Y., Vanapalli, S.K. and Wang, X.G. (2020), "Change in pore-size distribution of collapsible loess due to loading and inundating", *Acta Geotechnica*, **15**(3), 1081-1094. https://doi.org/10.1007/s11440-019-00815-9.

Wang, Y. and Wang, Y.L. (2017), "Liquefaction characteristics of gravelly soil under cyclic loading with constant strain amplitude by experimental and numerical investigations", *Soil Dyn. Earthq. Eng.*, **92**, 388-396. https://doi.org/10.1016/j.soildyn.2016.10.029.

Watanabe, Y., Lenoir, N., Otani, J. and Nakai, T. (2012), "Displacement in sand under triaxial compression by tracking soil particles on X-ray CT data", *Soils Found.*, **52**(2), 312-320. https://doi.org/10.1016/j.sandf.2012.02.008.

Yang, Z.H., Yue, Z.R. and Tai, B.W. (2021), "Investigation of the deformation and strength properties of fouled graded macadam materials in heavy-haul railway subgrade beds", *Constr. Build. Mater.*, **273**, 121778. https://doi.org/10.1016/j.conbuildmat.2020.121778.

Zhang, P.W. (2017), "Pore-structure model of geo-materials and micro-mechanics model for seepage", Ph.D. Dissertation, Tsinghua University, Beijing.

GC